Outgoing Longwave Flux Estimation: Improvement of Angular Modelling Using Spectral Information

N. Clerbaux *,1, S. Dewitte, L. Gonzalez, C. Bertrand,

B. Nicula, A. Ipe

Royal Meteorological Institute of Belgium, Department of Observations, Section Remote Sensing from Space, Avenue Circulaire 3, B-1180 Brussels, Belgium.

Abstract

A radiance–to–flux conversion is needed to estimate radiative fluxes at the top of the atmosphere from directional measurements made by broadband radiometers on satellites. Such a conversion is known to be one of the major sources of error in the resulting instantaneous shortwave and longwave fluxes. This paper analyzes the possibility to improve the radiance–to–flux conversion for the longwave radiation when spectral information about the radiation is available through a set of narrow–band measurements. The study is based on a database of spectral radiance fields at the top of the atmosphere built using radiative transfer computation. The analysis of this database shows that there exists a certain degree of correlation between the angular and the spectral behaviours of the radiation field. According to the type and the accuracy of the spectral information, this correlation allows a 25 % to 55 % reduction of the error introduced by the radiance–to–flux conversion with respect to a simple model that uses only broadband information. The method discussed in this paper might be used when broadband radiometer and spectral imager data are

available together like the combination of GERB and SEVIRI or the combination of CERES and MODIS.

Key words: atmosphere, clouds, infrared spectra, satellite measurement.

PACS: 92.60.Nv, 42.68.Ay, 95.30.Jx, 92.60.Jq

1 Introduction

Top–Of–the–Atmosphere (TOA) radiative fluxes are defined as the quantities of radiant energy leaving the Earth–atmosphere system. The radiant energy is usually separated into the *solar flux,* which corresponds to the reflection of the incoming solar radiation by the Earth–atmosphere system, and the *thermal flux* which is emitted by this system. The thermal flux is often referred to as *Outgoing Longwave Radiation (OLR*). In conjunction with the incoming solar flux, these fluxes form the components of the Earth Radiation Budget (ERB) at the TOA. Accurate estimation of these fluxes is of great importance in the fields of meteorological, climatological and more generally environmental studies.

These fluxes can be derived from data provided by broadband (BB) radiometers on satellite platforms which perform accurate measurements of solar and thermal radiances $L(\theta, \phi)$ [$\mathrm{Wm^{-2}sr^{-1}}$], where θ and ϕ are the zenith and azimuth angles of observation, respectively. In this case, the radiance must be

* Corresponding author. Tel.:+32 2 3730610. Fax:+32 2 3746788.
Email address: Nicolas.Clerbaux@oma.be (N. Clerbaux).

[1] Supported by ESTEC contract No. 13568/99/NL/GD

converted into the flux F, the integral over all the (θ, ϕ) directions

$$F = \int_{\theta=0}^{\frac{\pi}{2}} \int_{\phi=0}^{2\pi} L(\theta, \phi)\, cos(\theta)\, sin(\theta)\, d\theta\, d\phi. \tag{1}$$

For an isotropic radiance field, the radiance–to–flux conversion is trivial ($F = \pi L$). Unfortunately, the radiance field $L(\theta, \phi)$ in Eq. (1) is not isotropic and an accurate characterization of the anisotropy is needed to estimate the flux from the directional measurement. The Anisotropic Emission Factor (AEF) $R(\theta, \phi)$ is defined as the ratio of the equivalent Lambertian flux $\pi L(\theta, \phi)$ to the actual flux F

$$R(\theta, \phi) = \frac{\pi L(\theta, \phi)}{F}. \tag{2}$$

This equation is widely used to infer the flux F from the directional measurement $L(\theta, \phi)$ after characterization of the radiation field anisotropy $R(\theta, \phi)$ (Smith, G. L. et al., 1986; Suttles et al., 1989; Loeb et al., 2002).

For the Earth Radiation Budget Experiment (ERBE) (Barkstrom, 1984), a set of empirical curves $R(\theta)$ has been derived from satellite measurements for different latitude zones, seasons, surface types and cloud fractions (Suttles et al., 1989). After selection of the adequate curve, the radiance–to–flux conversion is trivial using Eq. (2). These curves $R(\theta)$ are not dependent on the azimuth angle ϕ because, on average, the thermal radiance is independent on the relative azimuth angle. As all the anisotropy models analyzed in this study share this symmetry, the angle ϕ is not indicated anymore hereafter. Nevertheless, recent studies showed that the azimuth dependency may be large in some conditions (Minnis and Khaiyer, 2000).

When narrow–band (NB) measurements $\{L_{nb}\}$ of the radiation, measured at

the same viewing angles, are available in addition to the BB measurement L, an alternative approach was proposed in Stubenrauch et al. (1993). In this approach, the AEF is directly estimated as a function of the BB and NB radiances $R(\theta) = R(\theta, L, \{L_{nb}\})$. It must be noted that, while spectral information is not available for the ERBE dataset, spectral information is available for all the following ERB missions: ScaRaB (Kandel et al., 1998), CERES (Wielicki et al., 1996), GERB (Harries and Crommelynck, 1999). As an alternative to this direct use of spectral information it is also possible to improve the empirical method by using more detailed scene identification. In this case spectral information may be used indirectly for example to estimate the cloud infrared emissivity (Loeb et al., 2002).

Several studies are devoted to the estimation of the thermal flux from a set of NB measurements in the thermal part of the spectrum. In these studies, the flux is usually directly estimated using regression on the NB radiances and thus the spectral (NB–to–BB conversion) and the angular (radiance–to–flux) modellings are performed in one step. The parameterizations are carried out using radiative transfer calculations with different atmospheric profiles. The first multispectral thermal flux estimation technique was used by Raschke et al. (1973) on data from the Nimbus 3 radiometer. Ellingson et al. (1989) proposed and validated (Ellingson et al., 1994) an estimation method using 4 of the 19 HIRS (High resolution InfraRed Sounder) NB measurements. Schmetz and Liu (1988) parameterized regressions to estimate the flux from the Meteosat water vapour and infrared channels. In these studies, the problem of the angular conversion is not isolated from the problem of the NB–to–BB conversion.

In this paper, we analyze how spectral information can be used to improve the radiance–to–flux conversion of broadband longwave radiance measurements.

This improvement is possible if and only if there exists a correlation between the spectral $L(\lambda)$ and angular $L(\theta, \phi)$ behavior of the radiation field. Unlike the previous studies, the broadband radiance is assumed to be measured by a broadband radiometer rather than estimated from NB measurements.

This work has been carried out in the frame of two ERB projects: the Earth Radiation Mission (Ingmann, 1997) and the Geostationary Earth Radiation Budget (GERB). For both, a broadband radiometer provides thermal radiance $L(\theta, \phi)$ that has to be converted into thermal flux F. For this conversion, spectral information is available respectively through the *ERM cloud imager* and the *Spinning Enhanced Visible and Infrared Radiometer Imager* (SEVIRI) (Schmetz et al., 2002).

2 Methodology

To address the correlation between spectral signature $L(\lambda)$ and the anisotropy $R(\theta)$, a large database [2] of spectral radiance fields $L(\theta, \lambda)$ was built using the *Santa Barbara DISORT Atmospheric Radiative Transfer* (SBDART) model (Ricchiazzi et al., 1998). The radiative transfer computations were performed at 431 wavelengths covering the thermal region $[2.5 - 100]$ μm and for 4622 realistic conditions of the Earth–atmosphere system. For each element in the database, the main inputs for the radiative transfer computations were:

- The *atmospheric profiles* of temperature, pressure, water vapour and ozone concentrations. These profiles are extracted from the TIGR–3 database

[2] The database and the related documentation are available at: http://gerb.oma.be/SpectralRadiancesDB.

(Chevallier et al., 2000) which is a representative set of 2311 profiles selected among a larger set of worldwide soundings.

- The *surface* emissivity and skin temperature. The emissivity is chosen randomly in the range $[0.85-1]$. The surface temperature is set randomly close to the temperature at the lower level in the profile. Nevertheless, due to solar heating, these temperatures may differ significantly in some conditions.
- The *cloud cover* is generated randomly. The cloud cover may contain up to 3 overlapping layers, each characterized by a random height, optical thickness, phase (water or ice) and drop size distribution. Half of the database (2311 elements) corresponds to cloud free conditions and the other half corresponds to the same conditions but with the addition of cloud cover.

To obtain realistic conditions, there exist some constraints on these inputs (for example a high level cloud is always constituted of ice particles). For each element in the database, the flux F, the radiance field $L(\theta = \{0°, 5°, ..., 85°\})$ and the AEF $R(\theta = \{0°, 5°, ..., 85°\})$ are computed.

Note that the database represents neither the anisotropy due to structured surfaces (Otterman et al., 1995) nor the anisotropy due to broken cloud fields (Naber and Weinman, 1984; Duvel and Kandel, 1984) because SBDART is a *plane–parallel* radiative transfer model. On the other hand, the database is representative of the anisotropy due to surface temperature, atmospheric constituents and due to stratiform cloud cover, including the strong anisotropy due to cold and semi–transparent clouds (*cirrus*).

Fig. (1) shows the scatter plots of the AEF $R(\theta)$ versus the thermal radiance $L(\theta)$ for the 4622 elements in the database at 3 different angles of observation:

- The scatter plot at $\theta = 0°$ (top) illustrates that, on average, the AEF at

nadir increases linearly with the radiance L. This is an effect of the increase of anisotropy for increasing surface temperature. The strong anisotropy observed over semi–transparent cold clouds is clearly visible in this figure. This scatter plot shows that, even using a plane–parallel radiative transfer model like SBDART, it is possible to generate TOA radiance fields with large dispersion in term of anisotropy.

- The scatter plot at $\theta = 50°$ (middle) indicates that, for this angle of observation, the R values are close to 1 and there is only a reduced anisotropic effect. Such a result was reported in numerous studies (Otterman et al., 1997; Stubenrauch et al., 1993) and also from satellite observations (Suttles et al., 1989). The oblique observation allows an easy and accurate estimation of the thermal flux.
- At grazing observation angle ($\theta = 75°$, bottom), the R values are usually smaller than 1 and decrease with increasing radiance L.

From the database, NB radiance is easily obtained by spectral convolution with the spectral sensitivity curve $S(\lambda)$ of the NB channel

$$L_{nb}(\theta) = \int_0^\infty L(\theta, \lambda) S(\lambda) d\lambda. \tag{3}$$

Measurement of NB radiance is usually done with instruments having poorer calibration than the BB measurement. For this reason, the NB radiances L_{nb} are altered in this study by adding a random calibration error with a Gaussian distribution that has a standard deviation of $\eta = 2\%$ of the mean radiance in the channel. This value was chosen as representative of state–of–the–art imager.

The database was split in two equal parts of 2311 elements. Half of the data is used to fit the models on the data (i.e. parameterize the regressions) while the second half is used to evaluate the performances of these models. For this, the RMS error ε (in Wm^{-2}) which is introduced in the flux by the radiance–to–flux conversion is evaluated. The relative error (in %) is also given.

3 Anisotropy models

First, a simple non–spectral model of the anisotropy is analyzed. Its performance will only serve to quantify the improvement obtained when using spectral information. Second, models of the anisotropy using spectral information in form of a single NB radiance will be presented and evaluated. Finally, we will discuss models based on multiple NB measurements.

3.1 Non–spectral model

From the different scatter plots of Fig. (1), a simple model for the AEF takes the linear form:

$$R(\theta, L) = c_0(\theta) + c_1(\theta)L(\theta). \tag{4}$$

For each viewing zenith angle $\theta = \{0°, 5°, 10°, ..., 85°\}$, the model is fitted on the database and the error $\varepsilon(\theta)$ is evaluated. The best fits are drawn on the scatter plots of Fig. (1) and the variation of $\varepsilon(\theta)$ according to θ is given on Fig. (2). This figure illustrates a local maxima of $\varepsilon(\theta)$ at nadir which appears as the worst observation angle within the $\theta = [0° - 65°]$ range. For this reason, our analysis is restricted to the nadir observation angle. If the radiance–to–flux

conversion can be improved at nadir using spectral information, we expect a similar improvement for viewing angles in the $\theta = [0° - 65°]$ range. For nadir observation, the non–spectral model (4) leads to a TOA flux error of $\varepsilon = 2.2$ % (4.63 Wm^{-2}). In the following, this value will be used as a reference to quantify the improvement obtained using spectral information.

3.2 Models using spectral information from one NB measurement

Radiance–to–flux conversion using information from a single NB radiance is of interest since the Earth observing BB radiometers often have a single NB window channel in addition to their BB channels. This is the case for the ScaRaB (window channel= $10.5 - 12.5$ μm) and CERES (window channel= $8 - 12$ μm) instruments. These were not designed to help in the radiance-to-flux conversion but rather to supplement the broadband measurements in better understanding the underlying physics (e.g. greenhouse effect...).

For the ScaRaB thermal radiance–to–flux conversion, Stubenrauch et al. (1993) introduced the concept of atmospheric pseudo–absorptance

$$A(\theta) = 1 - \frac{L(\theta)}{\frac{\sigma}{\pi} T_B(\theta)^4}. \tag{5}$$

where σ is the Stefan–Boltzmann constant and T_B the brightness temperature in the window channel of ScaRaB. Using a database of spectral radiance fields generated with the LOWTRAN–7 radiative transfer model, they suggested the fit $R(\theta) = 1 + (0.55 - e^{-cos\theta})A(\theta)$. Note that this method was not used for the operational ScaRaB data processing. The ERBE models were used for consistency.

The performance of the Stubenrauch approach was analyzed as a function of the NB radiance wavelength. For this, the NB radiance L_{nb} is estimated using Eq. (3) with a narrow ($\Delta\lambda = 0.1$ μm) rectangular filter $S(\lambda)$ centered at increasing wavelength. The NB radiance is then converted into brightness temperature T_B and the pseudo–absorptance is estimated using (5). The spectral model of the anisotropy

$$R(0^\circ) = c_o + c_1 A(0^\circ) \tag{6}$$

is then analyzed. Of course, the best fit coefficients c_0 and c_1 in Eq. (6) are dependent on the wavelength of the NB measurement. The top curve in Fig. (3) gives the error ε of the model (6) according to the wavelength used to estimate the pseudo–absorptance (the horizontal line at $\varepsilon = 2.2$ % corresponds to the non–spectral model). This figure indicates that the best performance is observed for NB measurements done in atmospheric transmission windows. Within the main window ($8 - 12$ μm), the shortest wavelength gives the best result. The minimal error ($\varepsilon = 1.73$ % or 3.65 Wm^{-2}) is observed at $\lambda = 8.6$ μm. This is an improvement (reduction of the error) of about 20 % in regard to the non–spectral model.

Bypassing the conversion to pseudo–absorptance (5), it is possible to obtain a slightly better radiance–to–flux conversion. To show this, the AEF at nadir is estimated directly as a third order regression on the BB and NB radiances

$$\begin{aligned} R(0^\circ) = {} & c_0 + c_1 L + c_2 L_{nb} + c_3 L^2 + c_4 L L_{nb} + c_5 L_{nb}^2 + \\ & c_6 L^3 + c_7 L^2 L_{nb} + c_8 L L_{nb}^2 + c_9 L_{nb}^3. \end{aligned} \tag{7}$$

This form is used as a general non-linear fit without particular physical meaning for the regression coefficients. The performance of this model according

to the wavelength of the NB measurement is displayed in Fig. (3). As for the Stubenrauch model, the best performance is obtained in the atmospheric windows. Close to $\lambda = 12$ μm, the performances of the 2 models are quite similar but at shorter wavelength the third order regression presents a significant improvement relative to use of the pseudo–absorptance. Discarding the $\lambda < 5$ μm region, the best performance ($\varepsilon = 1.62$ % or 3.41 Wm^{-2}) is observed at the same wavelength $\lambda = 8.6$ μm than for the pseudo–absorptance. Here, the improvement is about one quarter relative to the non–spectral model. Narrow–band radiance at $\lambda < 5$ μm can be used provided that it contains only thermal radiation. The narrow wavelength interval $[4.6, 4.9]$ μm (located between the CO_2 and water vapour absorption bands) appears to be very informative for the radiance–to–flux conversion ($\varepsilon = 1.31$ % or 2.76 Wm^{-2}). On the other side of the CO_2 absorption peak ($\lambda < 4.2\mu m$), the radiance–to–flux conversion error is about $\varepsilon = 1.43$ % (3.01 Wm^{-2}).

Models (6) and (7) were evaluated in the case of narrow ($\Delta\lambda = 0.1$ μm) rectangular spectral filter. Table (1) gives the error ε of the third order regression (7) when L_{nb} is provided by one of the 8 SEVIRI thermal channels. The errors in Table (1) are in good agreement with Fig. (3), therefore the spectral extension of the NB measurement seems not to impact on the spectral information.

The previous results were obtained supposing that the NB measurements are contaminated with a realistic $\eta = 2$ % Gaussian noise level. Fig. (4) shows a strong dependency of the angular conversion error ε according to the noise level η when the third order regression (7) is used. To obtain a significant spectral improvement, the NB measurement(s) must be done with a relatively well–calibrated device. In practice, for NB thermal measurements from weather satellites, a noise level/calibration error below $\eta = 2$ % can be expected.

3.3 Models using spectral information from multiple NB measurements

In this section, the improvement in the radiance–to–flux conversion is analyzed when information about the spectral signature $L(\lambda)$ is available through a set of NB measurements $\{L_{nb}\}$. The analysis is done for 3 different cases of spectral information: the ones provided by the SEVIRI and MODIS imagers and also when the entire spectral signature $L(\lambda)$ is known (*spectroradiometer*). Here, the large number of NB measurements (8 for SEVIRI, 16 for MODIS and 431 for the *spectroradiometer*) prohibits a direct use of these measurements in high order regressions. For instance, a third order regression on the 16 thermal radiances of MODIS contains about a thousand coefficients. For this reason, the spectral information is first projected on the principal components axis (PCA) and the anisotropy models are built as regressions on a restricted set of the principal components. This is just a linear transformation of the $\{L_{nb}\}$ set that allows exploitation of the same spectral information using a restricted number of input quantities in the regressions. The radiance–to–flux conversion error is not modified by such a transformation.

The SEVIRI case is of interest because the SEVIRI spectral information can be used during the radiance–to–flux conversion for the GERB data. The AEF is here dependent on the broadband radiance L and on the 8 NB SEVIRI thermal radiances: $L_{3.9\mu\mathrm{m}}, L_{6.2\mu\mathrm{m}}, L_{7.3\mu\mathrm{m}}, L_{8.7\mu\mathrm{m}}, L_{9.7\mu\mathrm{m}}, L_{10.8\mu\mathrm{m}}, L_{12.0\mu\mathrm{m}}, L_{13.4\mu\mathrm{m}}$. As explained above, these NB radiances were converted into 8 components $\{c_i\}$ using principal components analysis and the model of the anisotropy takes the form: $R(\theta) = R(\theta, L, c_1, c_2, ..., c_8)$. The estimation of the AEF at nadir $R(0^\circ)$ has been analyzed for different regression orders and for increasing numbers N of coefficients $\{c_i\} = \{c_1, c_2, ..., c_N\}$. The minimal radiance–to–flux conver-

sion error ($\varepsilon = 1.26$ % or 2.65 Wm^{-2}) is observed when using a third order regression on the BB radiance L and the $N = 7$ first components $\{c_i\}$. The spectral signature provided by the SEVIRI instrument allows to reduce the radiance–to–flux conversion error by about 43 % relative to the non–spectral model. Note that if the SEVIRI window channel at 3.9 μm is not used (because of possible contamination by solar reflected radiation), the error is just a bit larger ($\varepsilon = 1.31$ % or 2.76 Wm^{-2}).

The MODIS case is of interest because this spectral information might be used for the CERES data processing: these 2 instruments fly on the EOS Terra and Aqua satellites. The MODIS imager provides 16 NB measurements in the thermal part of the spectrum. The best radiance–to–flux conversion at nadir ($\varepsilon = 1.17$ % or 2.48 Wm^{-2}) is here observed using a third order regression on the BB radiance and the $N = 5$ first components $\{c_i\}$. Despite the fact that MODIS has twice as many channels as SEVIRI, the improvement in the spectral conversion is quite limited. This is explained by the fact that MODIS and SEVIRI provide measurements in the same parts of the thermal spectrum.

The database also allows to investigate the improvement that can be obtained when the entire spectral signature $L(\lambda)$ is available. This case study is of interest because it places a theoretical limit on the improvement using spectral information and also because infrared spectroradiometers are planned to fly in some future Earth observation missions, for instance the Fourier Transform Spectrometer of the ESA Earth Explorers EarthCARE mission. The analysis was done in the same manner as for SEVIRI and MODIS. The instrument is here supposed to provide 431 narrow radiance measurements between 2.5 and 100 μm. The need to project the spectral signature $L(\lambda)$ on the principal com-

ponent axis is obvious here: it is impossible to deal with high order regressions on such a large number of inputs. The best radiance–to–flux conversion is obtained using a second order regression on the $N = 13$ principal components $\{c_i\}$. In this case the angular conversion error for nadir observation reaches $\varepsilon = 1$ % (2.12 Wm^{-2}), which is just less than the half of the error of the non–spectral model.

4 Conclusions

In this paper, the possibility of improving the radiance–to–flux conversion for broadband thermal radiation using spectral information is addressed. This work is based on a database of spectral radiance fields $L(\theta, \lambda)$ at the top of the atmosphere. As the radiative transfer model (SBDART) used to build the database is a plane–parallel model, it is not possible to deal with the anisotropy due to broken cloud fields or structured surface. Nevertheless, the database is representative of the others sources of anisotropy, including the strong anisotropy observed for semi–transparent cirrus clouds.

Different case studies have outlined a weak correlation between spectral signature $L(\lambda)$ and angular behavior $L(\theta)$ for the thermal radiation field. This weak correlation can be exploited to improve the conversion into fluxes of the thermal radiances measured by broadband radiometers like CERES, ScaRaB or GERB. The improvement is quantified according to a simple non–spectral radiance–to–flux conversion model. The improvement is dependent on the number, the kind and the accuracy of the spectral measurements. Using only one NB measurement as spectral information, it was shown that this measurement should be done in an atmospheric transmission window and at the short-

est possible wavelength. The exploitation of spectral signature from multi-channel imagers like SEVIRI or MODIS allows a reduction of the radiance–to–flux conversion error of about 45 %. When the entire thermal spectrum $L(\lambda)$ is known, the analysis shows a possible reduction of the radiance–to–flux conversion error up to about 55 %. In the case of nadir observation, this corresponds to a reduction of the angular conversion error of 1.98 Wm^{-2} (SEVIRI) and 2.51 Wm^{-2} (entire spectrum).

It must be underlined here that the spectral information is not the only variable that can be exploited to obtain accurate thermal fluxes at the TOA from broadband radiance measurements. All information about surface temperature, atmospheric profiles of temperature and greenhouse gas concentrations (including water vapour) and about the cloud cover is useful to characterize the anisotropy at the top of the atmosphere and hence to improve the accuracy of the inferred thermal flux.

Acknowledgments. The authors are grateful to the CERES Inversion Group, NASA Langley Research Center, for all their constructive comments. They also would like to thank Konstantin Loukachine, Science Applications International Corp., Richard Allan, Hadley Center for Climate Prediction and Research, and an anonymous reviewer for critical review of this paper.

References

Barkstrom, B. R., 1984. The earth radiation budget experiment (ERBE). Bulletin of the American Meteorological Society 65, 1170–1186.

Chevallier, F., Chédin, A., Chéruy, F., Morcrette, J. J., 2000. TIGR-like atmo-

spheric profile databases for accurate radiative flux computation. Quarterly Journal of the Royal Meteorological Society 126, 777–785.

Duvel, J. P., Kandel, R. S., 1984. Anisotropy of longwave radiation emergent from a broken cloud field and its effect on satellite estimates of flux. Journal of Climate and Applied Meteorology 23, 1411–1420.

Ellingson, R. G., Yanuk, D. J., Lee, H. T., Gruber, A., 1989. A technique for estimating outgoing longwave radiation from HIRS radiance observations. Journal of Atmospheric and Oceanic Technology 6, 706–711.

Ellingson, R. G., Lee, H. T., Yanuk, D. J., Gruber, A., 1994. Validation of a technique for estimating outgoing longwave radiation from HIRS radiance observations. Journal of Atmospheric and Oceanic Technology 11, 357–365.

Harries, J. E., Crommelynck, D., 1999. The geostationary earth radiation budget experiment on MSG-1 and its potential applications. Advances in Space Research 24, 915–919.

Ingmann, P., 1997. The Earth Radiation Mission (ERM). In: Proc. of the Workshop on Synergy of Active Instruments in the Earth Radiation Mission. GKSS, Germany, pp. 47–50.

Kandel, R., Viollier, M., Raberanto, P., Duvel, J. P., Pakhomov, L. A., Golovko, V. A., Trishchenco, A. P., Mueller, J., Raschke, E., Stuhlmann, R., the ISSWG, 1998. The ScaRaB earth radiation budget database. Bulletin of the American Meteorological Society 79, 765–783.

Loeb, N. G., Smith, N. M., Kato, S., Miller, W. F., Gupta, S., Minnis, P., Wielicki, B. A., 2002. Angular distribution models for top–of–atmosphere radiative flux estimation from the Clouds and the Earth's Radiant Energy System instrument on the Tropical Rainfall Measuring Mission Satellite. Part I: Methodology. Journal of Applied Meteorology (submitted).

Minnis, P., Khaiyer, M. M., 2000. Anisotropy of land surface skin temperature

derived from satellite data. Journal of Applied Meteorology 39, 1117–1129.

Naber, P. S., Weinman, J. A., 1984. The angular distribution of infrared radiances emerging from broken fields of cumulus clouds. Journal of Geophysical Research 89, 1249–1257.

Otterman, J., Susskind, J., Brakke, T., Kimes, D., Pielke, R., Lee, T., 1995. Inferring the thermal-infrared hemispheric emission from sparsely-vegetated surface by directional measurements. Boundary-Layer Meteorology 74, 163–180.

Otterman, J., Starr, D., Brakke, T., Davies, R., Jacobowitz, H., Mehta, A., Chéruy, F., Prabhakara, C., 1997. Modeling zenith-angle dependence of outgoing longwave radiation: Implication for flux measurements. Remote Sensing of Environment 62, 90–100.

Raschke, E., Vonder Harr, T. H., Bandeen, W. R., Pasternak, M., 1973. The annual radiation balance of the earth-atmosphere system during 1969–70 from Nimbus 3 measurements. Journal of the Atmospheric Sciences 30, 341–364.

Ricchiazzi, P., Yang, S., Gautier, C., Sowle, D., 1998. SBDART: a research and teaching software tool for plane-parallel radiative transfer in the Earth's atmosphere. Bulletin of the American Meteorological Society 79, 2101–2114.

Schmetz, J., Liu, Q. 1988. Outgoing longwave radiation and its diurnal variation at regional scales derived from Meteosat. Journal of Geophysical Research 93, 11192–11204.

Schmetz, J., Pili, P., Tjemkes, S., Just, D., Kerkmann, J., Rota, S., Ratier, A., 2002. An introduction to Meteosat Second Generation (MSG). Bulletin of the American Meteorological Society 83, 977–992.

Smith, G. L., Green, R. N., Raschke, E., Avis, L. M., Suttles, J. T., Wielicki, B. A., Davies, R., 1986. Inversion methods for satellite studies of the Earth's

radiation budget: development and algorithms for the ERBE mission. Review of Geophysics 24, 407–421.

Stubenrauch, C. J., Duvel, J. P., Kandel, R. S., 1993. Determination of longwave anisotropic emission factors from combined broad- and narrowband radiance measurements. Journal of Applied Meteorology 32, 848–856.

Suttles, J. T., Green, R. N., Smith, G. L., Wielicki, B. A., Walker, I. J., Taylor, V. R., Stowe, L. L., 1989. Angular radiation models for earth-atmosphere system. Volume II– longwave radiation. Reference Publication 1184, NASA.

Wielicki, B. A., Barkstrom, B. R., Harrison, E. F., Lee, R. B., Smith, G. L., Cooper, J. E., 1996. Clouds and the earth's radiant energy system (CERES): An earth observing system experiment. Bulletin of the American Meteorological Society 77, 853–868.

WMO, 1996. Documentation of new cloud datasets. Document Version 1, International Satellite Cloud Climatology Project.

List of Figures

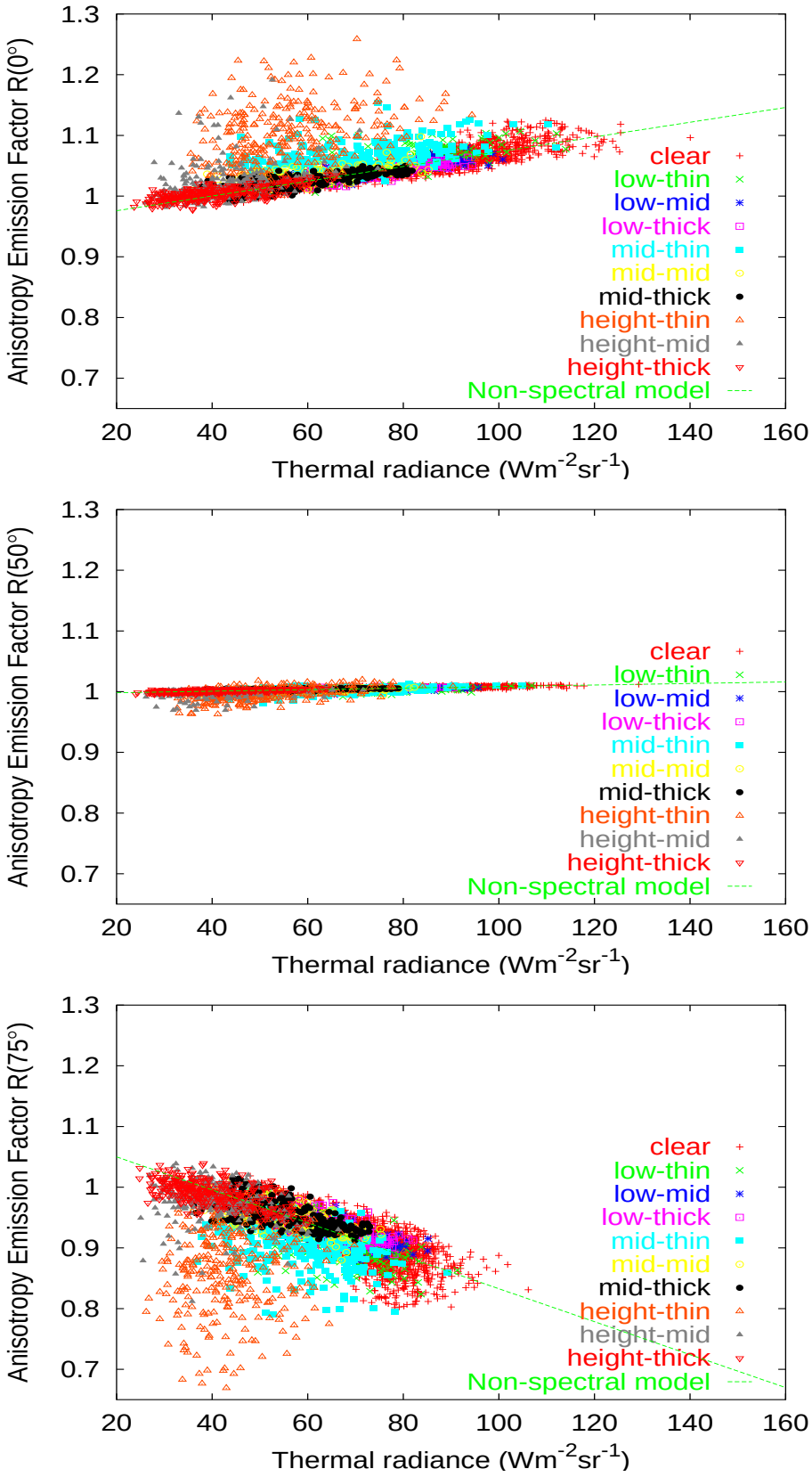

Fig. 1. Scatter plots of the AEF $R(\theta)$ versus the thermal radiance $L(\theta)$ for 3 angles of observation: $\theta = 0°$ (top), $\theta = 50°$ (center) and $\theta = 75°$ (bottom). The 4622 elements in the database are plotted using the ISCCP cloud classification (WMO, 1996).

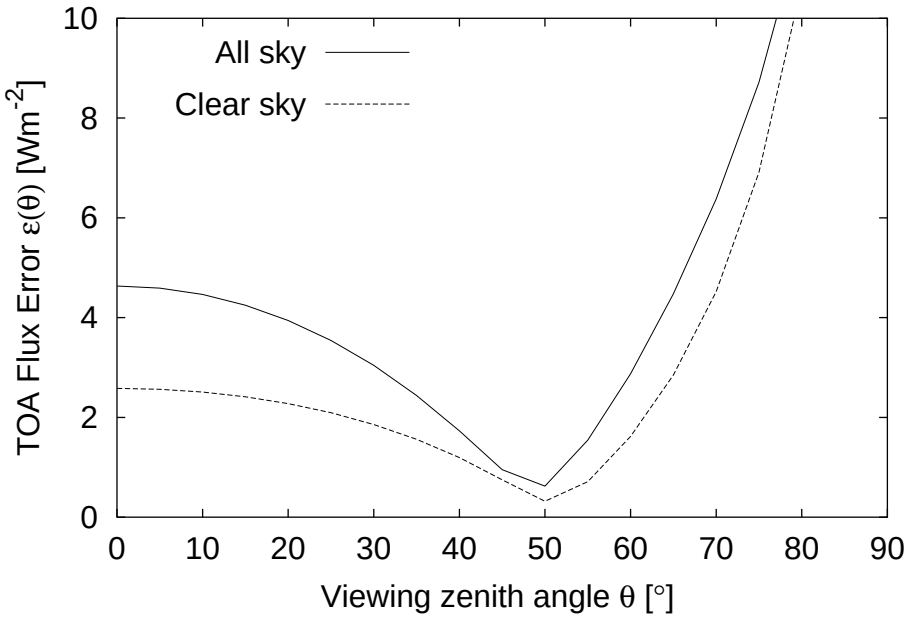

Fig. 2. Radiance–to–flux conversion error $\varepsilon(\theta)[\mathrm{Wm}^{-2}]$ versus the viewing zenith angle θ for the non–spectral model (4). The upper curve is for the entire database (clear–sky + cloudy conditions). The dashed curve is the error evaluated from the clear–sky subset.

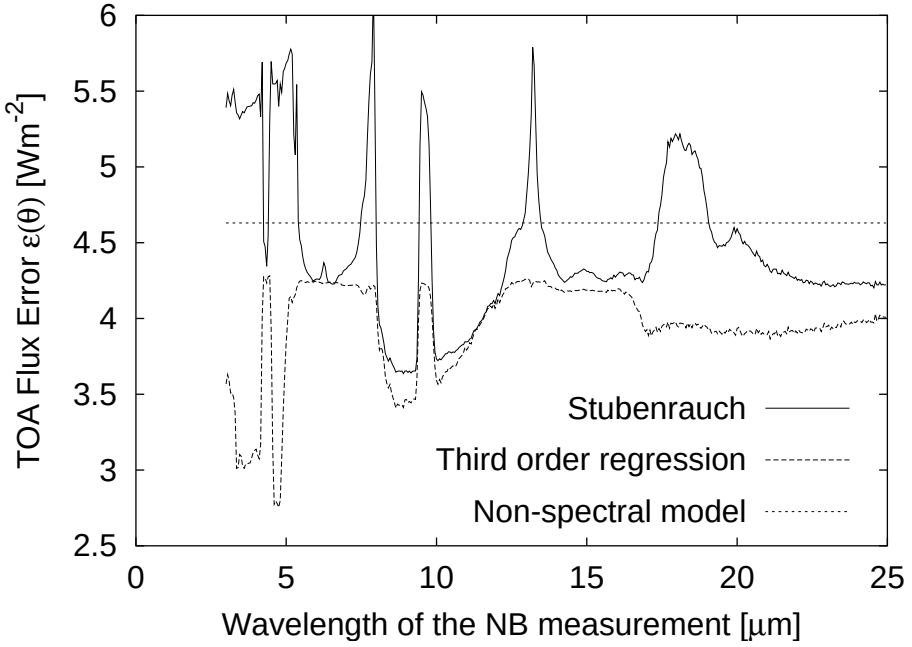

Fig. 3. Radiance–to–flux conversion error ε [Wm^{-2}] at nadir for the: non-spectral model (4), the pseudo–absorptance regression (6) and the third order regression (7). The error is dependent on the wavelength of the NB measurement.

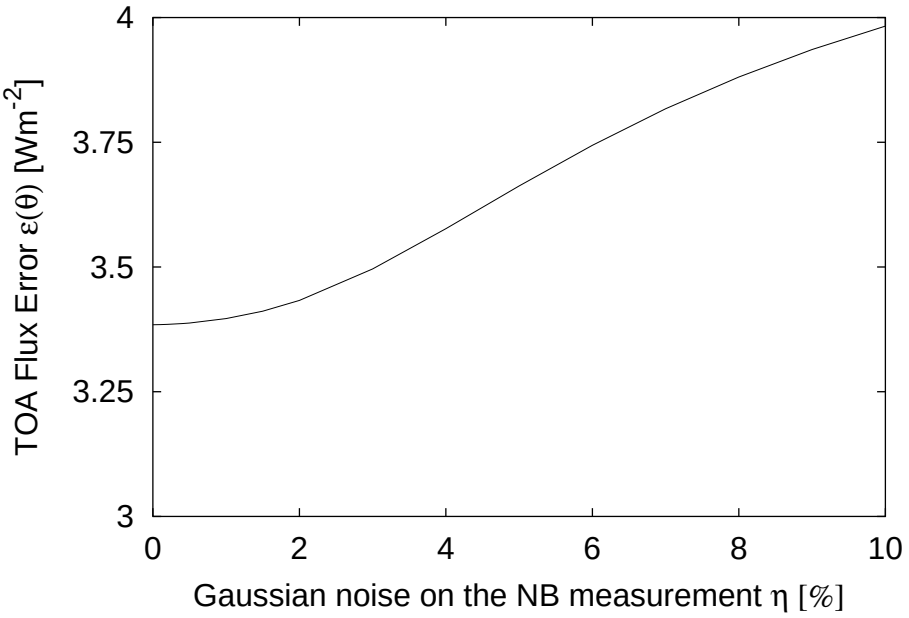

Fig. 4. Radiance–to–flux conversion error at nadir ε [Wm^{-2}] versus the noise level η on the SEVIRI 8.7 μm measurement when the AEF at nadir is estimated using the 3th order regression (7).

channel	type	ε [%]	ε [Wm^{-2}]
3.9μm	WIN	1.47	3.09
6.2μm	WV	2.01	4.23
7.3μm	WV	2.00	4.21
8.7μm	WIN	1.63	3.43
9.7μm	O_3	2.00	4.21
10.8μm	WIN	1.79	3.76
12.0μm	WIN	1.95	4.10
13.4μm	CO_2	2.02	4.26

Table 1
Radiance–to–flux conversion error at nadir ε in [%] and in [Wm^{-2}] when the AEF is estimated using the third order regression (7) on the BB radiance L and one of the 8 SEVIRI thermal radiances.